ACS Medicinal Chemistry Letters

pubs.acs.org/acsmedchemlett Letter

Structural and in Vitro Functional Characterization of a Menthyl TRPM8 Antagonist Indicates Species-Dependent Regulation

V. Blair Journigan,* David Alarcón-Alarcón, Zhiwei Feng, Yuanqiang Wang, Tianjian Liang, Denise C. Dawley, A. R. M. Ruhul Amin, Camila Montano, Wade D. Van Horn, Xiang-Qun Xie, Antonio Ferrer-Montiel, and Asia Fernández-Carvajal

Cite This: *ACS Med. Chem. Lett.* 2021, 12, 758−767

Read Online

ACCESS | Metrics & More | Article Recommendations | Supporting Information

ABSTRACT: TRPM8 antagonists derived from its cognate ligand, (−)-menthol, are underrepresented. We determine the absolute stereochemistry of a well-known TRPM8 antagonist, (−)-menthyl **1**, using VCD and 2D NMR. We explore **1** for its antagonist effects of the human TRPM8 (hTRPM8) orthologue to uncover species-dependent inhibition versus rat channels. (−)-Menthyl **1** inhibits menthol- and icilin-evoked Ca^{2+} responses at hTRPM8 with IC_{50} values of 805 ± 200 nM and 1.8 ± 0.6 μM, respectively, while more potently inhibiting agonist responses at the rat orthologue (rTRPM8 IC_{50} (menthol) = 117 ± 18 nM, IC_{50} (icilin) = 521 ± 20 nM). Whole-cell patch-clamp recordings of hTRPM8 confirm the **1** inhibition of menthol-stimulated currents, with an IC_{50} of 700 ± 200 nM. We demonstrate that **1** possesses ≥400-fold selectivity for hTRPM8 versus hTRPA1/hTRPV1. (−)-menthyl **1** can be used as a novel chemical tool to study hTRPM8 pharmacology and differences in species commonly used in drug discovery.

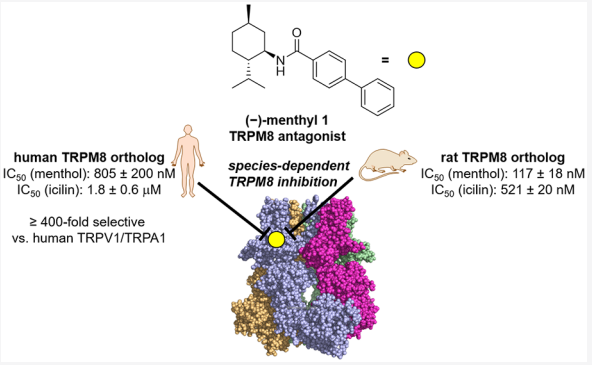

KEYWORDS: *TRPM8, menthol, antagonist, species, chemical regulation*

Transient receptor potential melastatin 8 (TRPM8) is a versatile target for chemotherapy-induced peripheral neuropathy,[1] neuropathic pain,[2] type 1 diabetes, and muscle wasting,[3] likely due to its ability to integrate distinct stimuli as a polymodal sensor. Menthol is the cognate ligand for TRPM8.[4] Its binding site has been explored in cryo-electron microscopy (cryo-EM) studies of collared flycatcher (avian) *Ficedula albicollis* TRPM8 ($TRPM8_{FA}$) bound to WS-12,[5] backed by radioligand displacement and mutagenesis data.[6] Many structurally disparate, non-menthol TRPM8 antagonist chemotypes have been reported, including several complexed with great tit (avian) *Parus major* TRPM8, implying a central binding cavity able to tolerate diverse scaffolds.[7] These recent advances suggest a mature drug discovery landscape; however, few menthol analogues with an antagonist profile are known (Figure 1), representing a gap in the literature for this chemotype. Such antagonists along with agonists of the same chemotype, will provide tools to identify the molecular mechanisms of ligand-induced channel gating. The structure of TRPM8 with an open ion permeation pathway remains elusive[8] despite known high-potency, menthol-derived agonists that could aid in its determination.[9] The structural mechanism underlying the coupling of antagonist binding and channel gating was recently described using a potent benzimidazole analogue TC-I 2014.[7] Complementary agonist derivatives within this series were not reported.[10]

(−)-Menthyl **1** (Figure 1) is a potent antagonist of rat TRPM8 (rTRPM8) in spectrofluorometric calcium (Ca^{2+}) flux assays using Fluo-4-AM as a fluorophore (IC_{50} vs 20 μM menthol = 20 ± 2 nM; IC_{50} vs 0.25 μM icilin = 50 ± 10 nM).[11] Its effects in the androgen-responsive prostate carcinoma cell line have also been explored.[15] We recently reported its activity using Fura-2-based calcium imaging of HEK-293 cells stably expressing hTRPM8 at an IC_{50} of 16 ± 1 μM, >300-fold lower than its reported IC_{50} at the rat orthologue, using a similar concentration of the agonist icilin (IC_{50} vs 0.5 μM icilin).[16] Differences in observed IC_{50} values for **1** may be dependent on TRPM8 orthologues (rat vs human) or different Ca^{2+}-sensitive fluorescent indicators.[17] The fluorescent Ca^{2+} assay is a standard functional assay for validating TRP-family ligands[4] and amenable to high throughput; however, Ca^{2+} is an indirect

Received: January 11, 2021
Accepted: March 26, 2021
Published: March 31, 2021

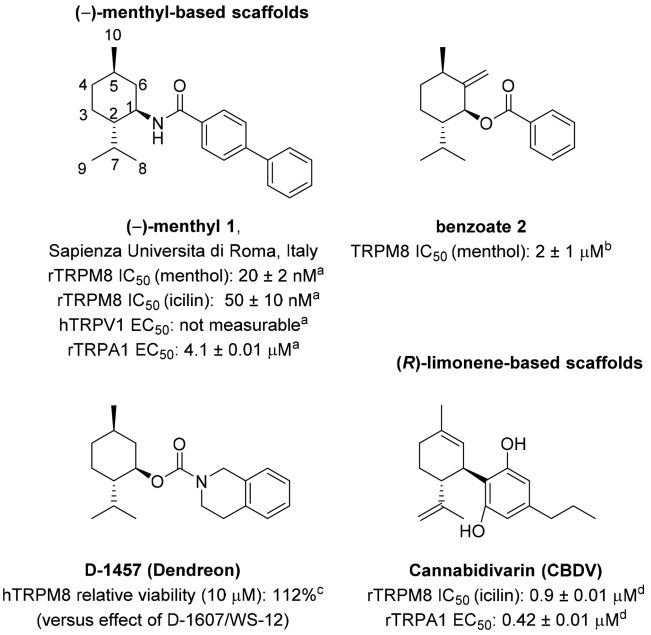

Figure 1. Monoterpene-derived TRPM8 antagonists. (a) Ref 11. (b) Ref 12, TRPM8 orthologue not specified. (c) Ref 13. (d) Ref 14.

signal indication of activity and does not offer real-time functional characterization of electrophysiology. Whole-cell patch-clamp measurements of **1** would validate both the nature of the functional effect and magnitude of antagonism.

In the same assay, benzoate **2** (Figure 1) has relatively low potency against menthol (100 μM) stimulated currents of TRPM8 (IC_{50} = 2 ± 1 μM), although the orthologue is not specified.[12] The antagonist effect of **D-1457** (Figure 1)[13] is only described at a single high concentration of 10 μM in cell viability assays. Indeed, various functional assays are used to explore antagonist activity of these menthol-based compounds, at times with minimal or incomplete data. Conversely, cannabidivarin (Figure 1) bears a limonene group similar to menthol and has defined pharmacology. However, this compound is a non-selective TRPM8 antagonist, with bifunctional TRPA1 agonist activity.[14] Well-characterized menthol-based antagonists are needed to serve as natural product TRPM8 probes and provide scaffolds as leads for drug discovery.

Results and Discussion. We first resynthesized and assigned absolute stereochemistry of the well-known TRPM8 antagonist (−)-menthyl **1** with VCD and 2D NMR, with special attention to the α-chiral amide, which was not described before. Our previous molecular dynamics (MD) studies suggest that configuration at this carbon positions the biphenyl moiety in the same region of the voltage-sensor-like domain (VSLD, transmembrane helices S1−S4) binding site as the methoxyphenyl moiety of agonist WS-12, with the 1′-phenyl ring extending into the floor of the pocket, toward the TRP helix.[16] Comparison with the bound pose of TC-I 2014 shows that the 1′-phenyl ring of **1** occupies a similar space in the TRPM8 binding site as the 5-(2-trifluoromethyl-phenyl) of TC-I 2014. This suggests that a second phenyl ring could be partly responsible for functional profile differences of these two menthol analogues.

Ortar et al. described the preparation of **1**[11] via (−)-menthylamine (1*R*,2*S*,5*R*)-2-isopropyl-5-methylcyclohexan-1-amine) using methodology by Schopohl and colleagues,[18] followed by EDCI/HOBt-assisted amidation. However, the absolute stereochemistry of (−)-menthylamine was not confirmed to be consistent with the structure reported by the latter group, who reported its X-ray crystal structure via incorporation into a caffeine complex.[19] We resynthesized (−)-menthylamine[18] starting from L-menthone **I-1** (Scheme 1). We prepared oxime **I-2** using standard conditions from **I-1** (95% yield), followed by Bouveault−Blanc reduction to **I-3** in quantitative yield. Oxime **I-2** and amine **I-3** were not purified to prevent exclusion of any minor isomers. GC-MS traces and ^{1}H NMR spectra of **I-2** and **I-3** indicate that these reactions afford minimal side product formation (Supporting Information (SI), Figures S1−S7). EDCI/HOBt-assisted coupling of **I-3** with 1,1′-biphenyl carboxylic acid afforded **1** in 76% yield, comparable to the reported yield (81%).[11]

The absolute stereochemical configuration of **1** was established by VCD[20] and ^{1}H, ^{13}C, gCOSY, NOESY, and gHSQCAD solution NMR experiments. The solvent-corrected IR and VCD spectra for (−)-menthyl **1** were obtained (SI, Figure S8). We performed a conformer search on the (1*R*,2*S*,5*R*) enantiomer of compound **1** using ComputeVOA from BioTools. We then optimized the 70 lowest energy conformers (8 kcal range from global minimum, SI, Figure S9) obtained with the MMFF94 force field and calculated IR and VCD frequencies using the B3LYP method and 6311Gdp basis set in Gaussian '09. Convolved spectra from the 20 lowest energy unique conformers were averaged using Boltzmann weighting from the energies obtained from optimization and plotted using a scaling factor of 0.983. We compared their Boltzmann summation with the observed spectra of (−)-menthyl **1** (Figure 2). After *X*-axis scaling of the computed spectra, there was strong correlation to the experimental of both IR and VCD with a neighborhood similarity (Sfg)[21] of 90.4 for IR and 78.6 for VCD and an enantiomeric similarity index (ESI)[21] of 70.8. Given this agreement, the absolute configuration of (−)-menthyl **1** was assigned as 1*R*,2*S*,5*R*.

Analysis of 2D NMR data including NOESY confirmed the correct relative stereochemistry (SI, Table S1, Figures S14−S17). Both data sets suggest chirality at the C1 position matching the reported structure,[11] for which stereochemical assignment is currently lacking in the literature. Our results also indicate that reduction favors formation of the desired amine, suggesting the isopropyl group provides sufficient steric bulk to

Scheme 1[a]

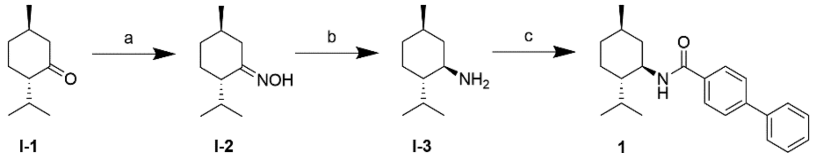

[a](a) NH_2OH, NaOH, EtOH/H_2O, rt, 95%; (b) Na^+, EtOH/toluene, reflux, quantitative; (c) 1,1′-biphenyl carboxylic acid, EDCI, HOBt, Et_3N, THF, 40 °C, 76%.

https://doi.org/10.1021/acsmedchemlett.1c00001
ACS Med. Chem. Lett. 2021, 12, 758−767

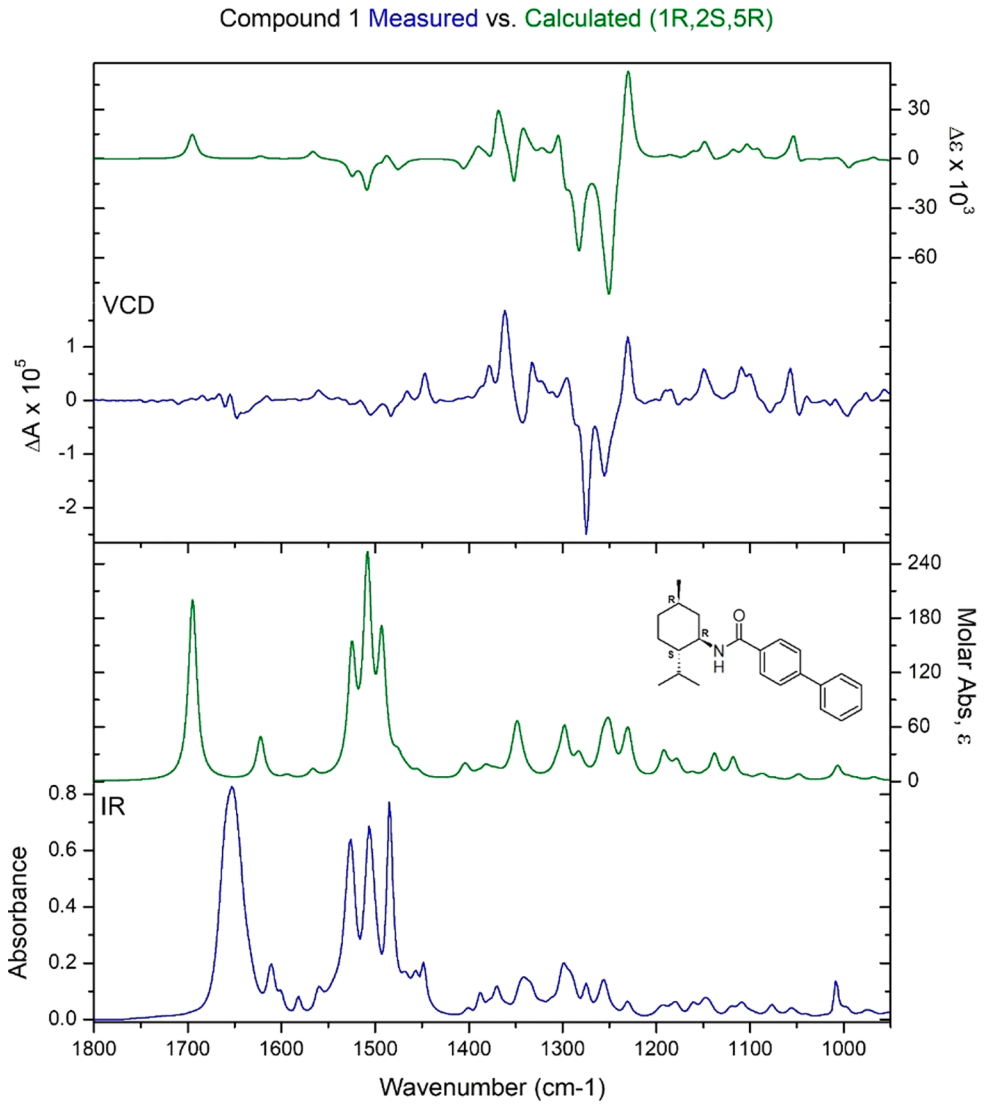

Figure 2. VCD (upper frame) and IR (lower frame) spectra observed (blue) for compound **1** (left axes) compared with Boltzmann-averaged spectra of calculated (green) conformations for the (1*R*,2*S*,5*R*) configuration (right axes).

confer stereoselectivity. Determining the stereochemistry at this position is crucial to explore agonist vs antagonist binding epitopes that could explain differences in functional activity because this chiral center determines orientation of the biphenyl moiety in the TRPM8 binding site.

To assess (−)-menthyl **1** for species-dependent inhibition of both menthol and icilin-mediated responses, we used calcium imaging at both human and rat TRPM8 carried out under the same conditions. We used the Fluo-4 NW probe that allows us to measure maximum responses after addition of the agonist, without saturating the signal, contrary to the Fura-2 probe. We first determined whether rat and human TRPM8 elicit different sensitivities to menthol and icilin in this assay. To this end, we obtained EC_{50} values of 81 ± 17 and 107 ± 8 μM for menthol stimulation of human and rat TRPM8 (Figures 3a and 4a), respectively. For icilin, we obtained EC_{50} values of 526 ± 24 nM and 554 ± 12 nM at human and rat TRPM8 (Figures 3a and 4a), respectively. These potencies are similar to those determined in CHO cells transfected with mouse TRPM8 using calcium imaging[22] and trigeminal neurons using patch-clamp electrophysiology.[4] Importantly, our measured EC_{50} values demonstrate equivalency for these agonists at both orthologues. In contrast, at hTRPM8 channels (−)-menthyl **1** inhibits both menthol and icilin responses at higher concentrations than the rat orthologue, with IC_{50} values of 805 ± 200 nM and 1.8 ± 0.6 μM, respectively (Figure 3b). At rTRPM8, **1** inhibits responses by both agonists more potently, with IC_{50} values of 117 ± 18 nM and 521 ± 20 nM against menthol and icilin stimulation, respectively (Figure 4b).

The antagonist effects of **1** (0.1, 1, 10 μM) against menthol stimulation at both human and rat TRPM8 are significantly different ($P < 0.001$ and $P < 0.0001$, two-way ANOVA followed by Bonferroni's test) (Figure 5). (−)-Menthyl **1** also exerts significantly different antagonist effects against icilin at both orthologues, at concentrations up to 10 μM ($P < 0.01$, two-way ANOVA followed by Bonferroni's test). Taken together, our data demonstrates that the potent antagonist effects of **1** observed at the rat orthologue result from species differences between rat and human TRPM8 channels. We propose that (−)-menthyl **1** can be used as a chemical tool to study species differences between rat and human TRPM8.

Other ligands with appreciable TRPM8 activity show species-dependent effects in vitro. The monoterpene eucalyptol activates hTRPM8 at an EC_{50} of 145.6 μM, although rodent

https://doi.org/10.1021/acsmedchemlett.1c00001
ACS Med. Chem. Lett. 2021, 12, 758−767

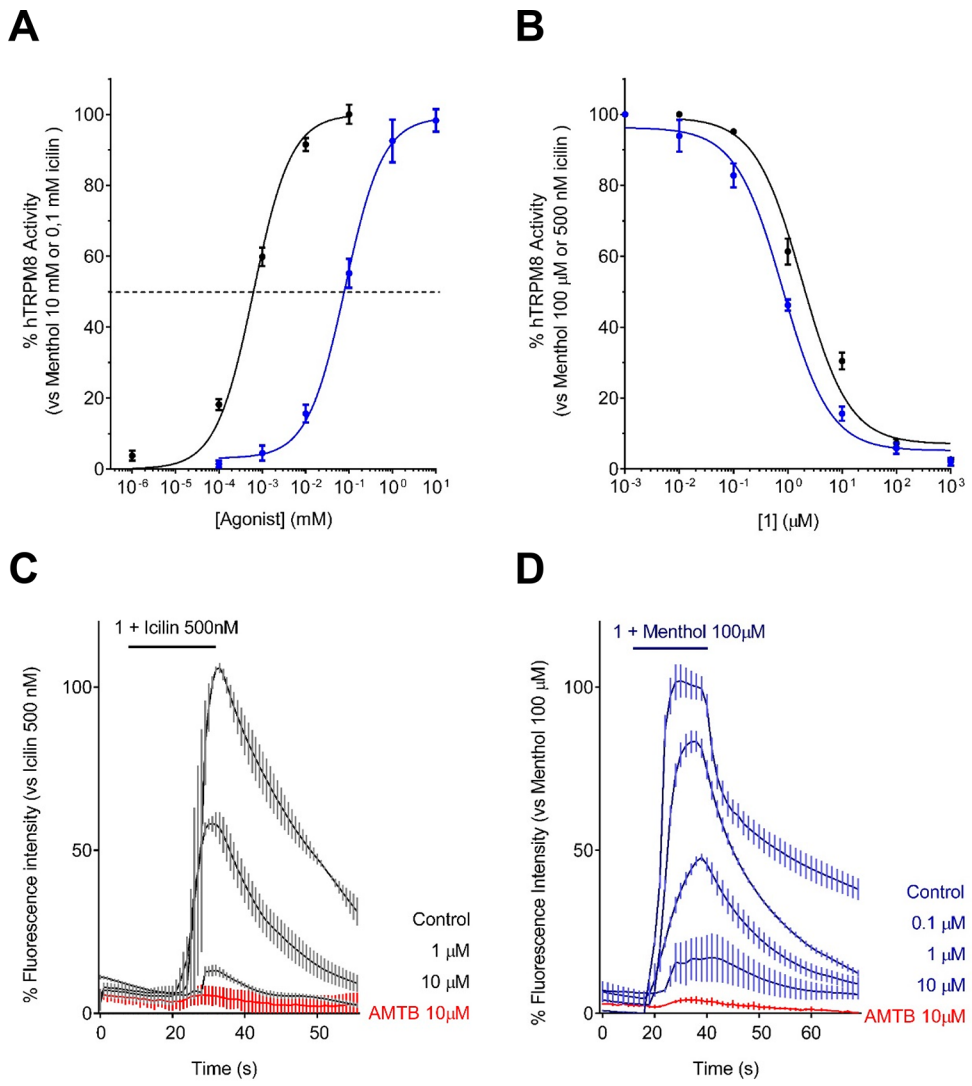

Figure 3. Characterization of hTRPM8 activity expressed in HEK293 cells by calcium imaging. (A) hTRPM8 activity evoked by icilin (black) or menthol (blue) (EC_{50} icilin = 526 ± 24 nM, EC_{50} menthol = 81 ± 17 μM). (B) hTRPM8 activity blocked by compound **1** using both agonists at its EC_{50}. (IC_{50} = 1.8 ± 0.6 μM for icilin activation, IC_{50} = 805 ± 200 nM for menthol activation). (C) Representative calcium traces for activity of hTRPM8 evoked by 500 nM icilin (control) in the presence of compound **1** from 0.1−10 μM. (D) Representative calcium traces for activity of hTRPM8 evoked by 100 μM menthol (control) in the presence of compound **1** from 0.1−10 μM. All data are expressed as mean ± SEM (n = 3, N = 3).

orthologues (rat and mouse) respond to eucalyptol only at higher EC_{50} values of 1.21 mM and 924.5 μM, respectively.[23] Menthol also displays species-dependent effects, activating chicken TRPM8 more potently than the mouse orthologue in both Ca^{2+} imaging and patch clamp assays.[24] On the other hand, icilin does not activate cTRPM8-expressing oocytes or HEK293 cells at a 10-fold higher concentration than required for a peak agonist response at rTRPM8.

Differential sensitivity among TRPM8 orthologues to icilin stimulation is attributed to Ala796 in the VSLD S3 helix, as Ala → Gly exchange confers avian sensitivity.[25] Yin et al. introduced the same mutation at the equivalent position (805) in $TRPM8_{FA}$ to confer icilin sensitivity and elucidated the icilin-bound structure via cryo-EM (PDB 6NR3).[5] Our previous MD studies of **1** carried out in the VSLD of our hTRPM8 homology model suggest that **1** binds in a pocket defined partially by Ala805.[16] This suggests residues responsible for differential sensitivities to compounds such as **1** may reside in the VSLD. On the other hand, sequence alignment of TRPM8 orthologues within the transmembrane domain, containing the VSLD, S5−S6 helices within the pore domain (PD), as well as the pore helix (PH) and TRP helix,[26] show that hTRPM8 differs from the rat orthologue at 10 unique positions. Eight of these residues are outside the VSLD binding site, in the upper S2 helix (Pro766, Val770, Ser773) and lower S2 helix (Val788). Remaining residues are distant to the binding cavity, in the loop connecting the PH and S6 helices (Gly921, Ala927, Thr932, His946) and the loop connecting the S6 and TRP helices (Thr985). Ser1007 (TRP helix) is the only point of differentiation close to the binding site for the two orthologues (Asn1007 in rTRPM8).

We previously reported MD simulations of **1** in our hTRPM8 model.[16] To explore the potential binding mode of **1** at rTRPM8 and provide structural context for our experimental data, we built a model of the rat orthologue using similar methodology as we reported previously.[16] Briefly, we built the rTRPM8 homology model based on the cryo-EM structure of $TRPM8_{FA}$ (PDB 6BPQ), which shares 80% sequence identity to rTRPM8. A calcium ion was placed in the VLSD, coordinating to Glu782, Gln785, Asn799, and Asp802, in agreement with our previous human model and calcium-bound structure of great tit *Parus*

https://doi.org/10.1021/acsmedchemlett.1c00001
ACS Med. Chem. Lett. 2021, 12, 758−767

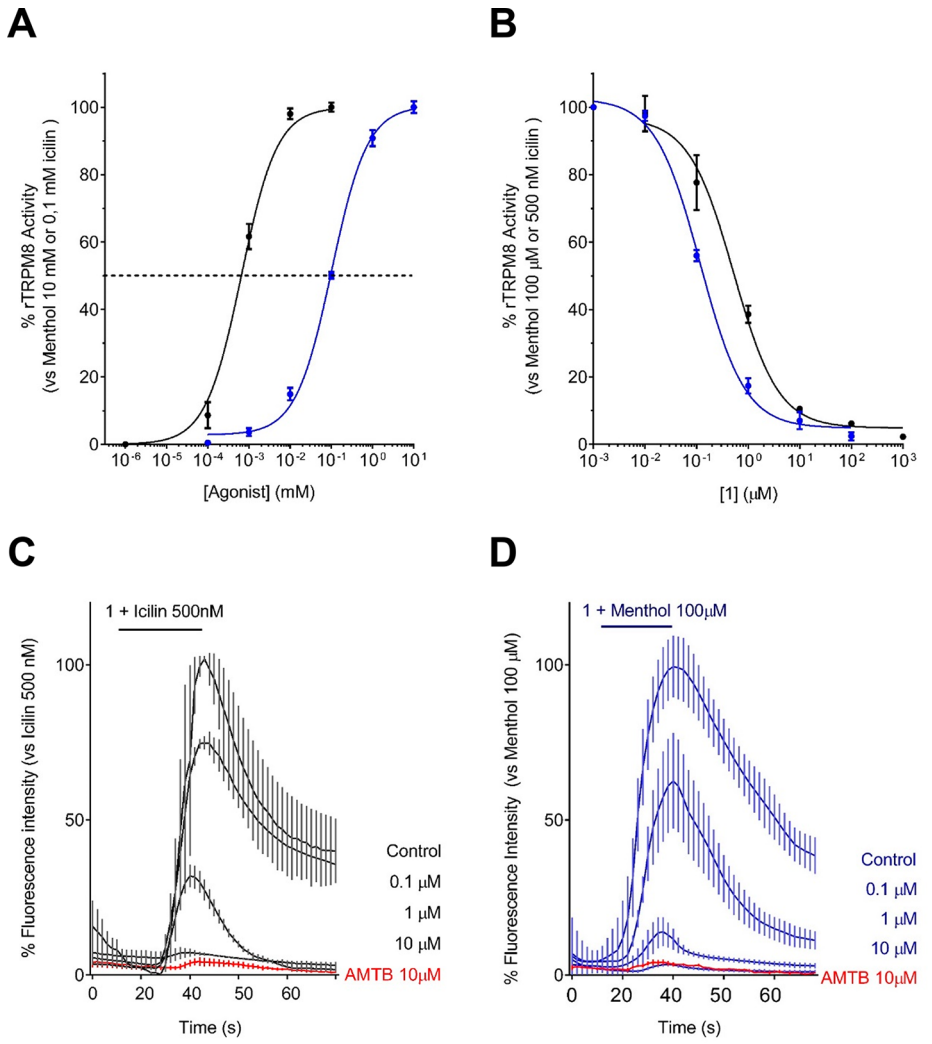

Figure 4. Characterization of rTRPM8 activity expressed in HEK293 cells by calcium imaging. (A) rTRPM8 activity evoked by icilin (black) or menthol (blue) (EC_{50} icilin = 554 ± 12 nM, EC_{50} menthol = 107 ± 8 μM). (B) rTRPM8 activity blocked by compound **1** using both agonists at its EC_{50}. (IC_{50} = 521 ± 20 nM for icilin activation, IC_{50} = 117 ± 18 nM for menthol activation). (C) Representative calcium traces for activity of rTRPM8 evoked by 500 nM icilin (control) in the presence of compound **1** from 0.1−10 μM. (D) Representative calcium traces for activity of rTRPM8 evoked by 100 μM menthol (control) in the presence of compound **1** from 0.1−10 μM. Data are expressed as mean ± SEM (n = 3, N = 3).

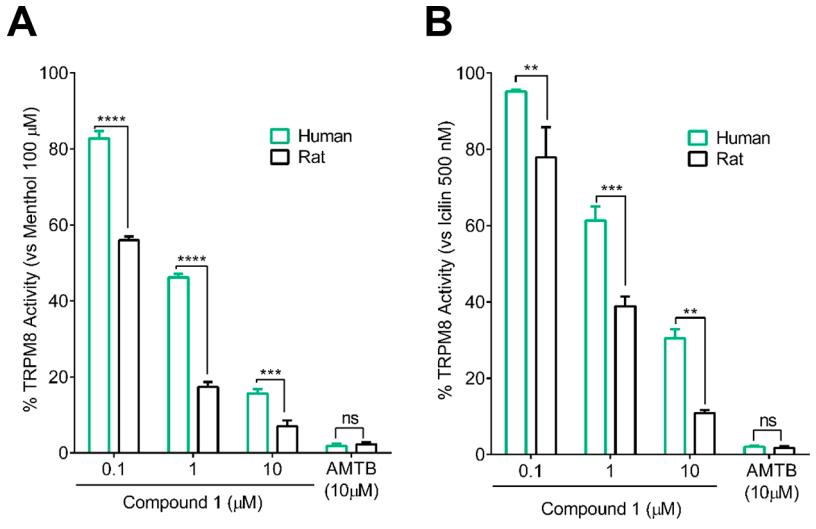

Figure 5. Comparative effect of compound **1** in hTRPM8 vs rTRPM8 activated by 100 μM menthol (A) or 500 nM icilin (B). Data are expressed as mean ± SEM (n = 3, N = 3). Data analyzed using two-way ANOVA followed by Bonferroni's post hoc test. $^{**}P < 0.01$, $^{***}P < 0.001$,**** $P < 0.0001$.

https://doi.org/10.1021/acsmedchemlett.1c00001
ACS Med. Chem. Lett. 2021, 12, 758−767

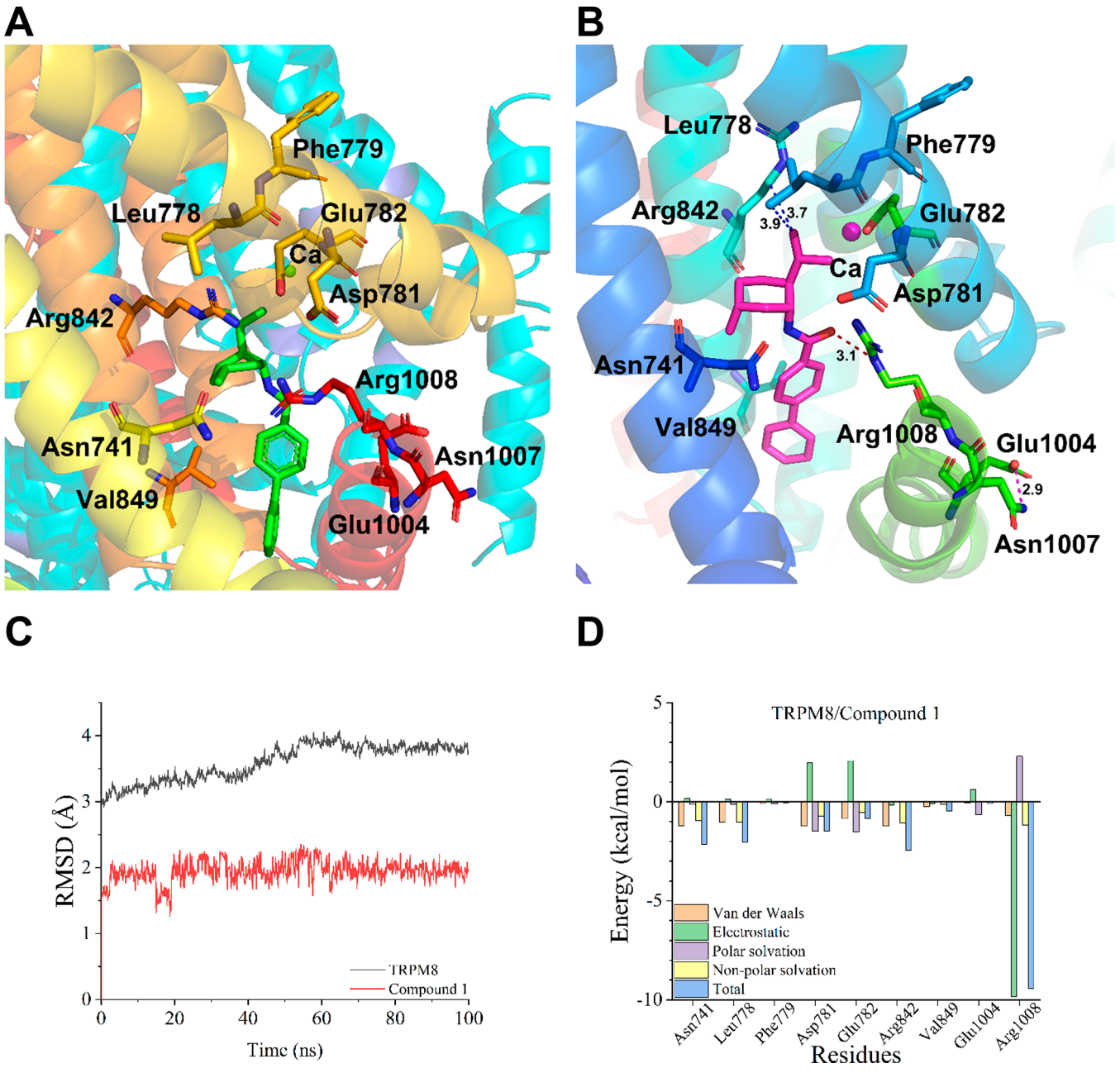

Figure 6. Convergence parameters of (−)-menthyl **1** and rTRPM8 during MD simulation. (a) Docking pose (pre-MD) of **1** in rTRPM8. (−)-Menthyl **1** is shown as green sticks. Important residues are shown as sticks. Individual helices are colored as follows: S1 (yellow), S2 (gold), S4 (orange), TRP helix (red). The Ca^{2+} ion (green) is shown in CPK representation. (b) Binding mode (post-MD) of **1** in rTRPM8 after 100 ns MD. (−)-Menthyl **1** is shown as magenta sticks. Important residues are shown as sticks. Individual helices are colored as follows: S1 (blue), S2 (light blue), S4 (cyan), TRP helix (green). The Ca^{2+} ion (magenta) is shown in CPK representation. (c) RMSD of **1** and rTRPM8 during MD simulation. (d) Energy decomposition of key residues in rTRPM8 that contributed to binding of **1**. Our rTRPM8 homology model was constructed using the cryo-EM structure of $TRPM8_{FA}$ (PDB 6BPQ) as a template.

major TRPM8.[7] We then performed 100 ns MD simulations for **1** in rTRPM8 using our reported protocol.[16] Our results show that both root-mean-square deviation (RMSD) of rTRPM8 (~2.0 Å) and (−)-menthyl 1 (~4.0 Å) kept stable after 60 ns during the simulation, indicating that the time scale of 100 ns is reasonable (Figure 6c). Interactions between **1** and some residues can be observed during the MD. For example, the carbonyl of **1** interacts with the guanidine moiety of a conserved Arg1008 (TRP helix, 3.1 Å) (Figure 6b). The isopropyl group of the (−)-menthyl core scaffold forms hydrophobic contacts with the backbone of Arg842 (S4, 3.7 Å) and Leu778 (S2, 3.9 Å). To explore the contribution of these residues to the binding of **1**, we decomposed the free energy using the MM/GBSA method (Figure 6d). From the energy decomposition, we found that Arg1008 contributed greatly to binding of **1**.

We then compared the predicted binding mode of **1** at rTRPM8 to our previous MD studies of this antagonist in our hTRPM8 homology model[16] via superimposition. As shown in Figure 7, **1** binds to rTRMP8 and hTRPM8 (gray) in a similar conformation, and key residues are oriented identically, with the exception of Phe779 and Ser/Asn1007. Arg1008 forms key interactions to **1** in both models, although at rTRPM8 this

https://doi.org/10.1021/acsmedchemlett.1c00001
ACS Med. Chem. Lett. 2021, 12, 758−767

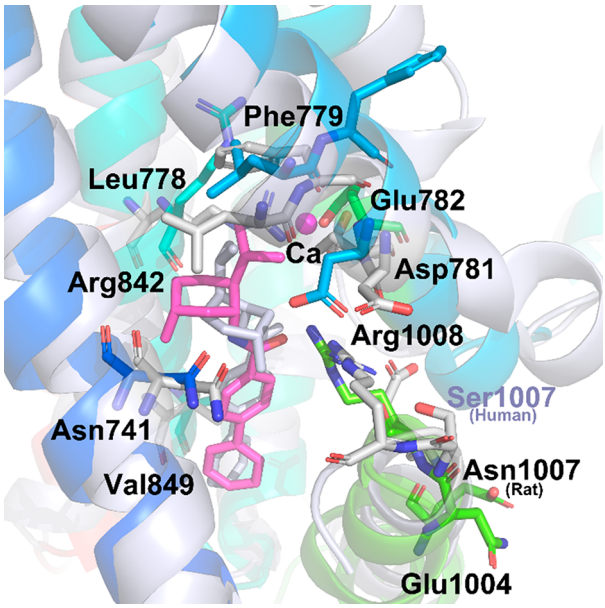

Figure 7. Superimposition of the binding mode (post-MD) of (−)-menthyl **1** in rTRPM8 (this work) and hTRPM8.[16] The MD pose of **1** and hTRPM8 is depicted in gray.

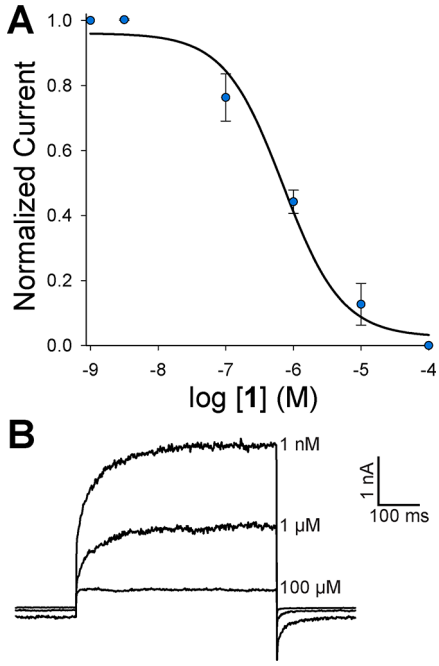

Figure 8. Whole-cell patch-clamp analysis of (−)-menthyl **1** inhibition of hTRPM8 validates species-dependent antagonism. (A) Normalized currents from menthol-evoked hTRPM8 show concentration-dependent inhibition. The IC_{50} of **1** against 500 μM menthol is 700 ± 200 nM (n = 3 cells). Data were recorded in transiently transfected HEK293 cells at +80 mV over a range of **1** concentrations (1 nM − 0.1 mM). Error bars indicate standard error of the mean. (B) Representative inhibition data from a single cell stimulated by 500 μM menthol and exposed to 1 nM, 1 μM, and 100 μM of compound **1**.

residue hydrogen-bonds to the **1** carbonyl via its guanidine moiety (Figure 6b), versus forming only hydrophobic contacts with the (−)-menthyl group via the three-carbon backbone at hTRPM8. We posit that at rTRPM8, Arg1008 is free to sample its conformational space due in part to the neighboring Asn1007 residue located 90° away, which forms hydrogen bonds to Glu1004 (2.9 Å). In contrast, at hTRPM8, the guanidine of Arg1008 is situated near Ser1007 (Figure 7), within 2.85 Å, and may anchor Arg1008 in position to form only hydrophobic interactions with **1**. These studies suggest that Ser/Asn1007 influences the binding pockets of both orthologues via spatial control of a conserved Arg1008 residue that forms key interactions with **1**.

Rodent and human TRPM8 also exhibit species differences in modulation by the accessory protein PIRT (phosphoinositide-interacting regulator of TRP). hPIRT attenuates menthol and cold-evoked hTRPM8 currents, whereas mPIRT increases the equivalent responses.[27] Innate differences in voltage-stimulated current densities have also been identified between orthologues.[27] Taken together, compounds such as **1** will be useful to identify mechanisms that underlie TRPM8 species-dependent effects and are anticipated to streamline drug discovery.

Whole-cell patch-clamp is the gold standard for deciphering ion channel molecular pharmacology, as it is a direct measurement of current flux through the channel, whereas Ca^{2+} flux assays are indirectly coupled to channel function, typically through a fluorophore. To validate our calcium fluorescent-based assays at hTRPM8, we performed electrophysiology of variable concentrations of **1** against 500 μM menthol (Figure 8) using our reported protocol.[16] In correlation with calcium imaging, whole-cell electrophysiological recordings showed that the antagonist activity of **1** at hTRPM8 is in the high nM range, with an IC_{50} value of 700 ± 200 nM. Notably, the IC_{50} value of **1** at hTRPM8 surpasses that of benzoate **2** (IC_{50}: 2 ± 1 μM)[12] in the same assay against the effect of 100 μM menthol, although the TRPM8 orthologue used was not reported. To our knowledge, **1** represents one of the most potent natural product-derived antagonists at hTRPM8 that possesses a strictly menthol chemotype.

Limited selectivity data are available for **1**. This antagonist is described as 200-fold selective for rTRPM8 versus rTRPA1 based on its measurable TRPA1 agonist activity (EC_{50}: 4.1 ± 0.01 μM). This may arise from the (−)-menthyl portion of **1** because menthol acts as an agonist at mouse TRPA1 (EC_{50}: 95 ± 15 μM)[28] and exerts significant TRPA1-mediated sensory effects in vivo.[29] Potential antagonist effects of **1** at this subtype were not determined.[11] In addition, **1** does not stimulate hTRPV1, although the concentration used in this assay was not disclosed, further arguing for antagonist studies at this subtype. Use of different orthologues (rTRPA1 and hTRPV1) for selectivity profiling of **1** may also pose further limitations. In light of sparse available selectivity data, the intrinsic (agonist) and antagonist activity of **1** at hTRPA1 and hTRPV1 was determined by Ca^{2+} flux experiments, using the standard agonists allyl isothiocyanate (AITC) and capsaicin and antagonists ruthenium red and capsazepine for each subtype, respectively. Experiments were conducted in HEK293 cells stably expressing each subtype, as we previously described.[16] We found **1** has negligible intrinsic (agonist) and antagonist activity in Ca^{2+} flux assays at both subtypes, at concentrations ≥400-fold higher than its hTRPM8 IC_{50} value (Table 1). Specifically, **1** did not activate either subtype >25% when normalized to the E_{max} concentration of AITC (300 μM) and capsaicin (3 μM) at all concentrations tested. Similarly, **1** did not inhibit either subtype >25% when challenged with the EC_{80} concentrations of AITC and capsaicin (10 and 0.1 μM, respectively). Thus, this antagonist demonstrates at least 400-fold selectivity for

https://doi.org/10.1021/acsmedchemlett.1c00001
ACS Med. Chem. Lett. 2021, 12, 758−767

Table 1. Intrinsic and Antagonist Functional Activities of (−)-Menthyl 1 at hTRPA1 and hTRPV1 Receptors, Determined in Ca^{2+} Flux Assays

compd	concentration tested (×TRPM8 IC_{50})	hTRPA1% activation ($n = 3$)[a]	hTRPA1% inhibition ($n = 3$)[b]	hTRPV1% activation ($n = 3$)[a]	hTRPV1% inhibition ($n = 3$)[b]
1,	66.7 μM (83-fold)	−0.83 ± 0.78	18.3 ± 2.66	1.3 ± 0.22	−3.6 ± 0.77
hTRPM8 IC_{50} (menthol): 805 ± 200 nM	133 μM (165-fold)	−0.20 ± 0.49	24.9 ± 1.67	3.6 ± 0.40	−7.44 ± 5.31
	200 μM (248-fold)	0.95 ± 0.80	18.7 ± 3.78	4.8 ± 0.20	−5.89 ± 2.96
	267 μM (332-fold)	2.1 ± 0.43	16.8 ± 3.20	4.57 ± 2.06	6.79 ± 6.71
	333 μM (414-fold)	3.4 ± 0.40	11.9 ± 3.10	7.9 ± 0.15	7.64 ± 4.47

[a]Data normalized to concentration corresponding to E_{max} value of TRPA1 and TRPV1 agonists AITC (300 μM) and capsaicin (3 μM), respectively. [b]Data normalized to EC_{80} of AITC (10 μM) and capsaicin (0.1 μM).

hTRPM8 versus other TRP subtypes when compared across uniform (human) orthologues. Although **1** does not achieve high potency at hTRPM8, it is well-characterized for its antagonist activity versus other menthol-based antagonists (Figure 1) and is ≥400-fold selective. These data suggest that **1** has worthy attributes to serve as a menthol-based antagonist probe to investigate TRPM8-mediated phenomena.

We present (−)-menthyl **1** as a well-characterized and selective menthol-based TRPM8 antagonist at the human orthologue for use as a chemical tool based on a menthol chemotype. Notably, (−)-menthyl **1** demonstrates a greater degree of TRPM8 inhibition in whole-cell patch-clamp electrophysiology assays measuring direct blockade of the channel than another reported menthol-based antagonist, benzoate **2**.[12] Previous studies describe **1** as a highly potent TRPM8 antagonist at the rat orthologue; however, we show species-dependent chemical regulation of rat versus human TRPM8 using this antagonist. (−)-menthyl **1** can be used as a tool to further study TRPM8 species differences and strongly supports that in vitro screening of ligands for TRPM8 activity should be performed using the human orthologue before conducting preclinical studies in rodents (rats). Initial in vitro calcium flux studies conducted only at rTRPM8 and subsequent in vivo studies in rats or mice may be misleading when considering the clinical translational potential of a chemical series. Similar cautions have been put forth for TRPA1[30] and TRPV1.[31] These studies should inform early drug discovery efforts to discover novel menthol-based TRPM8 antagonists as pharmacotherapies.

■ ASSOCIATED CONTENT

Supporting Information

The Supporting Information is available free of charge at https://pubs.acs.org/doi/10.1021/acsmedchemlett.1c00001.

Compound synthesis, functional assays, molecular modeling, GC-MS traces, NMR spectra, and VCD spectra (PDF)

Lay summary (PDF)

■ AUTHOR INFORMATION

Corresponding Author

V. Blair Journigan − *Department of Pharmaceutical Sciences, School of Pharmacy and Department of Biomedical Sciences, Joan C. Edwards School of Medicine, Marshall University, Huntington, West Virginia 25755, United States;* orcid.org/0000-0002-4582-5095; Email: journigan@marshall.edu

Authors

David Alarcón-Alarcón − *IDiBE: Instituto de Investigación, Desarrollo e innovación en Biotecnología Sanitaria de Elche, Universitas Miguel Hernández, 03202 Elche, Spain*

Zhiwei Feng − *Department of Pharmaceutical Sciences and Computational Chemical Genomics Screening Center, School of Pharmacy, NIDA National Center of Excellence for Computational Drug Abuse Research, and Drug Discovery Institute, University of Pittsburgh, Pittsburgh, Pennsylvania 15261, United States;* orcid.org/0000-0001-6533-8932

Yuanqiang Wang − *Department of Pharmaceutical Sciences and Computational Chemical Genomics Screening Center, School of Pharmacy, NIDA National Center of Excellence for Computational Drug Abuse Research, and Drug Discovery Institute, University of Pittsburgh, Pittsburgh, Pennsylvania 15261, United States*

Tianjian Liang − *Department of Pharmaceutical Sciences and Computational Chemical Genomics Screening Center, School of Pharmacy, NIDA National Center of Excellence for Computational Drug Abuse Research, and Drug Discovery Institute, University of Pittsburgh, Pittsburgh, Pennsylvania 15261, United States*

Denise C. Dawley − *Department of Pharmaceutical Sciences, School of Pharmacy, Marshall University, Huntington, West Virginia 25755, United States*

A. R. M. Ruhul Amin − *Department of Pharmaceutical Sciences, School of Pharmacy and Department of Biomedical Sciences, Joan C. Edwards School of Medicine, Marshall University, Huntington, West Virginia 25755, United States*

Camila Montano − *The School of Molecular Sciences, The Virginia G. Piper Center for Personalized Diagnostics, Biodesign Institute, and The Magnetic Resonance Research Center, Arizona State University, Tempe, Arizona 85287, United States*

Wade D. Van Horn − *The School of Molecular Sciences, The Virginia G. Piper Center for Personalized Diagnostics, Biodesign Institute, and The Magnetic Resonance Research Center, Arizona State University, Tempe, Arizona 85287, United States;* orcid.org/0000-0002-2493-5578

Xiang-Qun Xie − *Department of Pharmaceutical Sciences and Computational Chemical Genomics Screening Center, School of Pharmacy, NIDA National Center of Excellence for Computational Drug Abuse Research, and Drug Discovery Institute, University of Pittsburgh, Pittsburgh, Pennsylvania 15261, United States*

Antonio Ferrer-Montiel − *IDiBE: Instituto de Investigación, Desarrollo e innovación en Biotecnología Sanitaria de Elche, Universitas Miguel Hernández, 03202 Elche, Spain*

https://doi.org/10.1021/acsmedchemlett.1c00001
ACS Med. Chem. Lett. 2021, 12, 758−767

Asia Fernández-Carvajal − *IDiBE: Instituto de Investigación, Desarrollo e innovación en Biotecnología Sanitaria de Elche, Universitas Miguel Hernández, 03202 Elche, Spain*

Complete contact information is available at: https://pubs.acs.org/10.1021/acsmedchemlett.1c00001

Author Contributions

V.B.J. and D.A.A. contributed equally. The manuscript was written through contributions of all authors, who have approved the final version of the manuscript.

Notes

The authors declare no competing financial interest.

■ ACKNOWLEDGMENTS

We thank T. Voets (KU Leuven) for supplying the HEK293-hTRPM8 stable cell line. We thank T. Trejos and W. Feeney (West Virginia University) for GC-MS data and G. Rankin (Marshall University) for critical reading of the manuscript. This work was supported by the National Institutes of Health NIGMS U54GM104942−04 (V.B.J.) and R01GM112077 (W.V.H.), NIDA P30DA035778 (X-Q.X,); and by the Ministerio de Ciencia, Innovación y Universidades (MICIU) RTI2018-097189-B-C21 (A.F.M., A.F.C.).

■ ABBREVIATIONS

EDCI, *N*-(3-(dimethylamino)propyl)-*N*′-ethylcarbodiimide; HOBt, 1-hydroxybenzotriazole hydrate; gHSQCAD, gradient-enhanced heteronuclear single quantum coherence with adiabatic pulses

■ REFERENCES

(1) Gauchan, P.; Andoh, T.; Kato, A.; Kuraishi, Y. Involvement of increased expression of transient receptor potential melastatin 8 in oxaliplatin-induced cold allodynia in mice. *Neurosci. Lett.* **2009**, *458*, 93−95.

(2) Patel, R.; Goncalves, L.; Leveridge, M.; Mack, S. R.; Hendrick, A.; Brice, N. L.; Dickenson, A. H. Anti-hyperalgesic effects of a novel TRPM8 agonist in neuropathic rats: a comparison with topical menthol. *Pain* **2014**, *155*, 2097−2107.

(3) Bai, P.; Liu, Y.; Xue, S.; Hamri, G. C.; Saxena, P.; Ye, H.; Xie, M.; Fussenegger, M. A fully human transgene switch to regulate therapeutic protein production by cooling sensation. *Nat. Med.* **2019**, *25*, 1266−1273.

(4) McKemy, D. D.; Neuhausser, W. M.; Julius, D. Identification of a cold receptor reveals a general role for TRP channels in thermosensation. *Nature* **2002**, *416*, 52−58.

(5) Yin, Y.; Le, S. C.; Hsu, A. L.; Borgnia, M. J.; Yang, H.; Lee, S. Y. Structural basis of cooling agent and lipid sensing by the cold-activated TRPM8 channel. *Science* **2019**, *363*, eaav9334.

(6) Voets, T.; Owsianik, G.; Janssens, A.; Talavera, K.; Nilius, B. TRPM8 voltage sensor mutants reveal a mechanism for integrating thermal and chemical stimuli. *Nat. Chem. Biol.* **2007**, *3*, 174−182.

(7) Diver, M. M.; Cheng, Y.; Julius, D. Structural insights into TRPM8 inhibition and desensitization. *Science* **2019**, *365*, 1434−1440.

(8) Gruss, F. Hot new structures of the cold sensor, TRPM8, reveal insights into the fundamentals of cold perception and adaptation. *Cell Calcium* **2020**, *85*, 102112.

(9) Bharate, S. S.; Bharate, S. B. Modulation of thermoreceptor TRPM8 by cooling compounds. *ACS Chem. Neurosci.* **2012**, *3*, 248−267.

(10) Parks, D. J.; Parsons, W. H.; Colburn, R. W.; Meegalla, S. K.; Ballentine, S. K.; Illig, C. R.; Qin, N.; Liu, Y.; Hutchinson, T. L.; Lubin, M. L.; Stone, D. J., Jr; Baker, J. F.; Schneider, C. R.; Ma, J.; Damiano, B. P.; Flores, C. M.; Player, M. R. Design and optimization of benzimidazole-containing transient receptor potential melastatin 8 (TRPM8) antagonists. *J. Med. Chem.* **2011**, *54*, 233−247.

(11) Ortar, G.; De Petrocellis, L.; Morera, L.; Moriello, A. S.; Orlando, P.; Morera, E.; Nalli, M.; Di Marzo, V. (−)-Menthylamine derivatives as potent and selective antagonists of transient receptor potential melastatin type-8 (TRPM8) channels. *Bioorg. Med. Chem. Lett.* **2010**, *20*, 2729−2732.

(12) LeGay, C. M.; Gorobets, E.; Iftinca, M.; Ramachandran, R.; Altier, C.; Derksen, D. J. Natural-Product-Derived Transient Receptor Potential Melastatin 8 (TRPM8) Channel Modulators. *Org. Lett.* **2016**, *18*, 2746−2749.

(13) Natarajan, S. K.; Moreno, O.; Graddis, T. J.; Duncan, D.; Laus, R.; Chen, F. Compositions and methods using small molecule Trp-p8 modulators for the treatment of diseases associated with Trp-p8 expression. Word Patent WO2005020897A2, 2005.

(14) De Petrocellis, L.; Ligresti, A.; Moriello, A. S.; Allara, M.; Bisogno, T.; Petrosino, S.; Stott, C. G.; Di Marzo, V. Effects of cannabinoids and cannabinoid-enriched Cannabis extracts on TRP channels and endocannabinoid metabolic enzymes. *Br. J. Pharmacol.* **2011**, *163*, 1479−1494.

(15) De Petrocellis, L.; Ligresti, A.; Schiano Moriello, A.; Iappelli, M.; Verde, R.; Stott, C. G.; Cristino, L.; Orlando, P.; Di Marzo, V. Non-THC cannabinoids inhibit prostate carcinoma growth in vitro and in vivo: pro-apoptotic effects and underlying mechanisms. *Br. J. Pharmacol.* **2013**, *168*, 79−102.

(16) Journigan, V. B.; Feng, Z.; Rahman, S.; Wang, Y.; Amin, A.; Heffner, C. E.; Bachtel, N.; Wang, S.; Gonzalez-Rodriguez, S.; Fernandez-Carvajal, A.; Fernandez-Ballester, G.; Hilton, J. K.; Van Horn, W. D.; Ferrer-Montiel, A.; Xie, X. Q.; Rahman, T. Structure-Based Design of Novel Biphenyl Amide Antagonists of Human Transient Receptor Potential Cation Channel Subfamily M Member 8 Channels with Potential Implications in the Treatment of Sensory Neuropathies. *ACS Chem. Neurosci.* **2020**, *11*, 268−290.

(17) Bootman, M. D.; Rietdorf, K.; Collins, T.; Walker, S.; Sanderson, M. Ca^{2+}-sensitive fluorescent dyes and intracellular Ca^{2+} imaging. *Cold Spring Harb. Protoc.* **2013**, *2013*, 83−99.

(18) Schopohl, M. C.; Bergander, K.; Kataeva, O.; Fröhlich, R.; Waldvogel, S. R. Synthesis and Characterization of Enantiomerically Pure Menthylamines and Their Isocyanates. *Synthesis* **2003**, *2003*, 2689−2694.

(19) Schopohl, M. C.; Siering, C.; Kataeva, O.; Waldvogel, S. R. Reversible enantiofacial differentiation of a single heterocyclic substrate by supramolecular receptors. *Angew. Chem., Int. Ed.* **2003**, *42*, 2620−2623.

(20) He, Y.; Wang, B.; Dukor, R. K.; Nafie, L. A. Determination of absolute configuration of chiral molecules using vibrational optical activity: a review. *Appl. Spectrosc.* **2011**, *65*, 699−723.

(21) Polavarapu, P. L.; Covington, C. L. Comparison of experimental and calculated chiroptical spectra for chiral molecular structure determination. *Chirality* **2014**, *26*, 539−552.

(22) Andersson, D. A.; Chase, H. W.; Bevan, S. TRPM8 activation by menthol, icilin, and cold is differentially modulated by intracellular pH. *J. Neurosci.* **2004**, *24*, 5364−5369.

(23) Caceres, A. I.; Liu, B.; Jabba, S. V.; Achanta, S.; Morris, J. B.; Jordt, S. E. Transient Receptor Potential Cation Channel Subfamily M Member 8 channels mediate the anti-inflammatory effects of eucalyptol. *Br. J. Pharmacol.* **2017**, *174*, 867−879.

(24) Pertusa, M.; Rivera, B.; Gonzalez, A.; Ugarte, G.; Madrid, R. Critical role of the pore domain in the cold response of TRPM8 channels identified by ortholog functional comparison. *J. Biol. Chem.* **2018**, *293*, 12454−12471.

(25) Chuang, H. H.; Neuhausser, W. M.; Julius, D. The super-cooling agent icilin reveals a mechanism of coincidence detection by a temperature-sensitive TRP channel. *Neuron* **2004**, *43*, 859−869.

(26) Yin, Y.; Wu, M.; Zubcevic, L.; Borschel, W. F.; Lander, G. C.; Lee, S. Y. Structure of the cold- and menthol-sensing ion channel TRPM8. *Science* **2018**, *359*, 237−241.

(27) Hilton, J. K.; Salehpour, T.; Sisco, N. J.; Rath, P.; Van Horn, W. D. Phosphoinositide-interacting regulator of TRP (PIRT) has opposing

effects on human and mouse TRPM8 ion channels. *J. Biol. Chem.* **2018**, *293*, 9423−9434.
(28) Karashima, Y.; Damann, N.; Prenen, J.; Talavera, K.; Segal, A.; Voets, T.; Nilius, B. Bimodal action of menthol on the transient receptor potential channel TRPA1. *J. Neurosci.* **2007**, *27*, 9874−9884.
(29) Lemon, C. H.; Norris, J. E.; Heldmann, B. A. The TRPA1 Ion Channel Contributes to Sensory-Guided Avoidance of Menthol in Mice. *eNeuro* **2019**, *6*, 0304-19.2019.
(30) Chen, J.; Kang, D.; Xu, J.; Lake, M.; Hogan, J. O.; Sun, C.; Walter, K.; Yao, B.; Kim, D. Species differences and molecular determinant of TRPA1 cold sensitivity. *Nat. Commun.* **2013**, *4*, 2501.
(31) Garami, A.; Shimansky, Y. P.; Rumbus, Z.; Vizin, R. C. L.; Farkas, N.; Hegyi, J.; Szakacs, Z.; Solymar, M.; Csenkey, A.; Chiche, D. A.; Kapil, R.; Kyle, D. J.; Van Horn, W. D.; Hegyi, P.; Romanovsky, A. A. Hyperthermia induced by transient receptor potential vanilloid-1 (TRPV1) antagonists in human clinical trials: Insights from mathematical modeling and meta-analysis. *Pharmacol. Ther.* **2020**, *208*, 107474.

https://doi.org/10.1021/acsmedchemlett.1c00001
ACS Med. Chem. Lett. 2021, 12, 758−767